






Studying the Mechanical Behavior and Strengthening of RCSACC after Exposure to Elevated Temperatures

Estudio del comportamiento mecánico y refuerzo del RCSACC tras su exposición a temperaturas elevadas

Jean Jacques Kouadjo Tchekwagep ¹, Yiping Qiu ², Shifeng Huang ³, Shoude Wang ³, and Xin Cheng ³

ABSTRACT

Rapid calcium sulfoaluminate cement concrete (RCSACC) has received increased attention of late because it can be manufactured with less CO₂ emissions than ordinary Portland cement. In previous studies, RCSACC performed poorly when subjected to elevated temperatures, to which fiber-reinforced concrete (FRC) is a potential alternative. This study investigated the impact of incorporating two types of fibers, *i.e.*, copper-plated steel microfilament (CPM) and shear corrugated steel (SC), on the engineering, mechanical, and microstructural features of RCSACC after exposure to elevated temperatures. Pore size distribution, microstructure, and mechanical properties were tested after exposure to temperatures of 100, 200, and 300 °C. The content of each type of fibers represented 1% of the concrete. The results showed that the mechanical properties were affected by the addition of either type of steel fibers. Adding CPM or SC steel fibers could ensure an adequate resistance of RCSACC when exposed to high temperatures, in addition to improving its residual mechanical behavior, spalling resistance, and ductility after heating. Steel fibers contribute to enhancing both mechanical properties and resistance to heating effects. However, adding steel fibers also appears to increase microstructure damage with heat, reduce workability, entrap air and water, and reduce cracking related to drying shrinkage.

Keywords: mechanical properties, rapid calcium sulfoaluminate cement, copper-plated microfilament fibers, shear corrugated fibers, shrinkage

RESUMEN

Últimamente, el hormigón de cemento sulfoaluminato de calcio rápido (RCSACC) ha recibido una mayor atención porque puede fabricarse con menos emisiones de CO₂ que el cemento Portland ordinario. En estudios anteriores, el RCSACC presentó un mal desempeño cuando se sometió a temperaturas elevadas, para lo cual el hormigón reforzado con fibra (FRC) es una potencial alternativa. Este estudio investigó el impacto de la incorporación de dos tipos de fibras, *i.e.*, microfilamento de acero chapado en cobre (CPM) y acero corrugado (SC), en las características de ingeniería, mecánicas y microestructurales del RCSACC tras su exposición a temperaturas elevadas. Se probaron la distribución del tamaño de los poros, la microestructura y las propiedades mecánicas tras la exposición a temperaturas de 100, 200 y 300 °C. El contenido de cada tipo de fibras representaba el 1 % del hormigón. Los resultados mostraron que las propiedades mecánicas se vieron afectadas por la adición de cualquiera de los dos tipos de fibras de acero. La adición de fibras de acero CPM o SC podría garantizar una resistencia adecuada del RCSACC cuando se expone a altas temperaturas, además de mejorar su comportamiento mecánico residual, su resistencia al desconchado y su ductilidad después del calentamiento. Las fibras de acero contribuyen a mejorar tanto las propiedades mecánicas como la resistencia a los efectos del calentamiento. Sin embargo, la adición de fibras de acero también parece aumentar el daño a la microestructura con el calor, reducir la trabajabilidad, atrapar el aire y el agua, y reducir el agrietamiento relacionado con la contracción por secado.

Palabras clave: propiedades mecánicas, cemento de sulfoaluminato cálcico rápido, fibras de microfilamentos recubiertos de cobre, fibras onduladas de cizallamiento, contracción

Received: March 8th, 2023

Accepted: June 13th, 2024

¹ Ph.D. in Materials Science, University of Jinan, China. Affiliation: Lecturer, Shandong Provincial Key Laboratory of Preparation and Measurement of Building Materials, University of Jinan, China. Email: mse_wanggg@ujn.edu.cn

² Master's Student, University of Jinan, China. School of Materials Science and Engineering, University of Jinan, China. Email: 1019488037@qq.com

³ Postdoctoral Fellow, Hong Kong University of Science and Technology, China. Ph.D. in Materials Science, Wuhan University of Technology, China. Affiliation: Professor, Shandong Provincial Key Laboratory of Preparation and Measurement of Building Materials, University of Jinan, China. Email: mse_huangsf@ujn.edu.cn

⁴ Ph.D. in Materials Science and Engineering, Wuhan University of Technology, China. Affiliation: Professor, School of Materials Science and Engineering, University of Jinan, China. Email: mse_wangsd@ujn.edu.cn

⁵ Ph.D. in Materials Science, Wuhan University of Technology, China. Affiliation: Professor, Shandong Provincial Key Laboratory of Preparation and Measurement of Building Materials, University of Jinan, China. Email: chengxin@ujn.edu.cn



Introduction

Ordinary Portland cement concrete (OPCC) has been adopted in multiple projects around the world, making it the most widely used material on Earth (Chang *et al.*, 2020). The content of OPCC consists of Portland cement (PC), coarse aggregate, water, and sometimes an admixture (Cheng *et al.*, 2020). Experts do not consider OPCC to be an environmentally friendly material, since its production and manufacture releases a large portion of the world's overall CO₂ emissions (Venkatesh and Wasim, 2011). In this vein, the development and implementation of rapid calcium sulfoaluminate cement (RCSAC) constitute an encouraging option to decrease carbon dioxide emissions, which account for 7% of the global levels in the cement industry alone. Depending on its performance, RCSAC has several applications. Since the 1970s, cement research in China has managed to produce different types of calcium sulfoaluminate (CSA) cement, which are categorized as the *third cement series*. The advantage of their large-scale production lies in an abundance of resources and the reduced research funding required from the Chinese government (Li *et al.*, 2020, 2021; Michels *et al.*, 2016). Thus, China has gradually applied third-series cement in multiple engineering projects. Both China and India have successfully managed to use this binder to build waterproof pipes (Afroughsabe *et al.*, 2017; Augusto *et al.*, 2019).

RCSAC is mainly composed of ye'elimite (C₄A₃Š) (Afroughsabe *et al.*, 2016; Wang *et al.*, 2020). Increasing the ye'elimite content results in a faster early strength. As the largest and most widely used material in China and India, RCSACC is increasingly being used in current construction projects (Kohoutková *et al.*, 2017). When using this material, many issues can arise, such as those involving safety and sustainable development (Cheng *et al.*, 2020). Materials made with a cement base are generally weak in tension, including RCSACC (Barreto *et al.*, 2019; Chalioris *et al.*, 2018). Cracks appear when RCSACC is heated to high temperatures, as shown by Azzabi *et al.* (1993) and Bjegović *et al.* (2015). Moreover, it may crack when exposed to elevated temperatures, resulting in reduced mechanical properties (Tanyildizi and Yonar, 2016). A solution to this issue could be the addition of shear corrugated (SC) or copper-plated microfilament (CPM) fibers, aiming to increase the properties of RCSACC when exposed to heat (Aguilar *et al.*, 2015; Aravinthan *et al.*, 2018). Fibers have been shown to decrease early-age shrinkage by enhancing the cohesion between the concrete matrices (sand, cement, coarse aggregate, water, and fibers) (Li, 2019). There is ongoing research on the use of fiber in concrete materials, with the aim of reducing the damage inflicted by elevated temperatures on infrastructure. The effectiveness of using fibers depends on the type of fiber used, its elastic modulus, and its aspect ratio (Hong *et al.*, 2017).

The purpose of this article is to investigate the effect of SC and CPM on the behavior of RCSACC after exposure to elevated temperatures. In previous studies, we have

assessed the dehydration effects of increased temperature (Cheng, Huang, *et al.*, 2020a, 2020b). No other works have evaluated the impact of CPM and SC fibers on the features of RCSACC. A fiber content of 1% was used, and 24 RCSACC mixes were made with a 0.4 water-to-cement ratio. Mechanical properties were assessed after exposure to elevated temperatures. SEM and 3D microscopy were employed to explore the microstructural properties of the RCSACC samples used.

Test raw materials

Rapid calcium sulfoaluminate cement

For all preparations, we utilized RCSAC produced by China United Cement Jining Co. Ltd. (Shandong, China). Table 1 presents its chemical composition.

Table 1. Composition of the RCSAC used

Oxide compositions	Weight%	Mineralogical phase compositions	Weight%
CaO	45.2	C ₂ S	18
Al ₂ O ₃	17.5	C ₄ A ₃ Š	60
SO ₃	15.7	C ₁₁ A ₇ F	4.4
SiO ₂	9.19	CaSO ₄	9.9
Fe ₂ O ₃	2.50	2.5	4.5
MgO	1.90	1.9	Fluorescence
TiO ₂	0.7	0.7	
K ₂ O	0.4	0.4	Others
Na ₂ O	0.4	0.4	3.2
Specific gravity (g/cm ³) 3.1		Specific surface (m ² /kg) 450	

Source: Authors

Table 2 presents the aggregate used in this study (crushed limestone and silica sand).

Table 2. Physical properties of the aggregates

Aggregate type	Maximum size aggregate (mm)	Water absorption	Specific gravity	Fineness modulus
Fine aggregate	4.75	1.1	2.65	2.9
Coarse aggregate	19	0.96	2.74	

Source: Authors

We employed CPM and SC fibers with aspect ratios of 26.5 and 69.4, respectively. Figure 1 shows these fibers, and Table 3 lists their characteristics.

Table 3. Properties of the steel fibers

Type and shape of fiber	Length L (mm)	Diameter D (mm)	Aspect ratio L/D	Density (g/cm ³)	Tensile strength (N/mm ²)
Copper-plated microfilament (CPM)	13.3	0.5	26.6	7.8	2300
Shear corrugated (SC) fiber	37.5	0.54	69.4	7.8	1050

Source: Authors

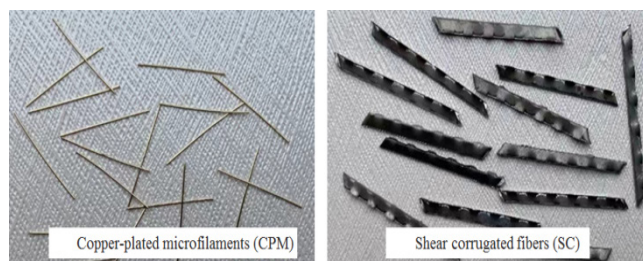


Figure 1. Two kinds of steel fibers

Source: Authors

RCSACC preparation

Table 4 shows the slump of the RCSACC-CPM and RCSACC-SC preparations. In this work, we established 18 ± 2 cm as the acceptable slump value. After they were produced, the preparations were placed in the molds. Three samples were prepared for each temperature range. After one day, the samples were demolded and cured at 23 ± 2 °C (Gashti et al., 2020) for 672 hours. Then, they were left exposed in the lab for 125 h.

Table 4. Mix proportions of the fiber-reinforced concrete mixes

Mixture ID	W/C	Water	RCSA	FA	CA
		(kg/m ³)			
RCSACC 12 cm (slump)	0.4	216	540	622	727
1% retarder					
RCSACC-CPM					
CPM fiber volume fraction (%)					
0 1 1	0.4	216	540	622	727
12.5 cm (slump)					
1% retarder					
RCSACC-SC					
SC fiber volume fraction (%)	0.4	216	540	622	727
0 1 1					
12 cm (slump)					
1% retarder					

CPM: copper-plated microfilament fibers; SC: shear corrugated fibers.

Source: Authors

Then, the samples were placed in an electric furnace for heating at the rate of 4°C/min until they reached the target temperature, which was maintained for 4 h. This time proved to be enough to ensure the effective decomposition of all the important ingredients forming the RCSAC, i.e., AFT and Al(OH)₃ (Aluko et al., 2020; Bai et al., 2019).

Testing properties

Measuring the drying shrinkage

It is important to study the shrinkage behavior of expanded RCSACC for a more pertinent assessment. The Chinese standard GB-T50082 was used for evaluating the drying shrinkage of the concrete. Three specimens of each composition, with a size of 100 × 100 × 515 mm, were used to measure the shrinkage. The test piece was poured and maintained in a molded state, at a temperature of 28 ± 0.5 °C and 75% relative humidity. While this state was maintained, the effective length was measured, and the shrinkage rate was determined. The test result was calculated based on the average of the three specimens.

Surface image analysis

Surface images of the different RCSACC specimens were captured using a high-resolution optical zoom camera. Afterwards, the images underwent a treatment process, with the aid of a software named GelAnalyzer (Ahmed, 2021). Crack images were generated and drawn with the aid of vellum paper, and the Lightroom software helped to clear up the images. Following that, a description of the crack areas was constructed in the ImageJ software.

Ultrasonic testing

Waveform variations can serve as an important indicator of the internal characteristics of each sample, both before and after conditioning (Błaszczyszki et al., 2012; Mehta et al., 2006). In the context of ultrasonic testing, the frequency was set at 50 kHz, and the input voltage at 10 V.

Flexural strength-displacement

In accordance with GB/T50081-2019, the national testing standard for the physical and mechanical properties of concrete, this experiment used specimens with side lengths of 100 × 100 × 400 mm. We calculated the flexural strength (ff) by means of the formula $ff = Fl/bh^2$, where ff is the flexural strength; F is the failure load of the specimen (N); l is the span between supports (mm); b is the cross-section width of the specimen (mm); and h is the cross-section height of the specimen.

Compressive strength

This experiment used standard cube specimens with a side length of 100 × 100 × 100 mm. The percent strength variation (Q) as the temperature increased was defined as follows:

$Q = \left| \frac{\sigma - \sigma_0}{\sigma_0} \right| \times 100\%$. In this formula, σ_0 is the compressive strength of the specimens at ambient temperature (20 °C), and σ is the strength of the sample after thermal exposure.

Mercury porosimetry (MIP) and micromorphology (SEM) analysis

We tested the different samples using MIP and SEM tools, aiming to observe the pore distribution and microcrack patterns. Small squares with a side length of 10 ± 1 mm were taken from the crushed sample for MIP testing. For the SEM observation, we used a diamond saw to create small sections (typically 1-2 cm), focusing on areas of interest (e.g., cracks and fiber-matrix interfaces). Using a vacuum oven, we made sure that the samples were completely dry to prevent water vapor interference during imaging. Finally, we placed the samples in the vacuum chamber of a QUANTAFEG250 field emission scanning electron microscope (SEM) for analysis.

Results

Workability

In accordance with ASTM C143, we determined the workability of the fresh RCSACC-CMP, RCSACC-SC, and RCSACC samples. RCSACC's fresh workability was seen to be negatively affected by the addition of CPM and SC fibers. Figure 2 shows the slump of each blend.

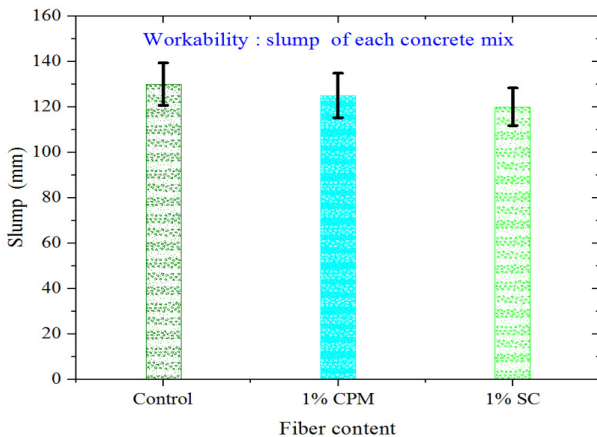


Figure 2. Workability of RCSACC mixes
Source: Authors

Fiber characteristics play an important role in how the fibers blend into the matrix. In this study, the workability observed was found to be relatively consistent across all samples. Moreover, fibers tend to reduce workability because of their large specific area, which adheres some of the available cement paste, thereby reducing the availability of excess paste to reduce inter-particle friction. As for the slump test results, the 1% value obtained more or less meets the workability goal for the fresh RCSACC mixture, as set at the beginning of the study.

Free shrinkage

In the control samples (RCSACC), thin cracks appeared approximately 2 h 30 min after casting, spreading all over the samples. This is a consequence of strong water absorption during setting, which continues throughout curing. In the case of the RCSACC samples with a 1% CMP or SC fiber content, the emergence of the first crack took more than 10 h. Thus, the emergence period for the RCSACC-CMP and RCSACC-SC samples was four times longer than that of the control sample. The free shrinkage strain can be substituted into the following formula to find the stress in the reinforcements:

$$f_{sc} = \frac{\varepsilon_{cs} E_s}{1 + \frac{\alpha A_s}{A_c}} \quad (1)$$

where f_{sc} stands for the stress in the reinforcements, as caused by the shrinkage (N/mm^2); $\alpha = \frac{E_s}{E_{cm}}$, with E_s and E_{cm} being the modulus of elasticity of the fiber and concrete – it is a non-dimensional term that accounts for the non-uniform distribution of stress in the concrete section due to cracking, with values of 0.184 for RCSACC-CMP and 0.123 for RCSACC, and it indicates the shrinkage-related stress in the reinforcements and the relationship between the reinforcement used and the stress in RCSACC; A_s stands for the cross-sectional area of the fiber reinforcement; and A_c stands for the cross-sectional area of the concrete. The tension for both types of reinforced fibers is negligible and could be applicable when the RCSACC is partially restrained by reinforcements. As for the free shrinkage strain, RCSACC must be stretched to cover the strain caused by shrinkage. The restraint values obtained for RCSACC-CMP and RCSACC-SC are greater than the partial restraint regardless of the fiber content. This suggests that the addition of the steel fibers is not helpful to RCSACC exposed to elevated temperatures. Figure 3 illustrates the cracking on the three specimens as the sample shrinks. Here, Figure 3c presents the case of RCSACC-SC, wherein very thin, slight cracks appeared. The assessment focused on the width and area covered by the cracking. This manifestation of cracks is the reason why water was observed on the surface of the different samples.

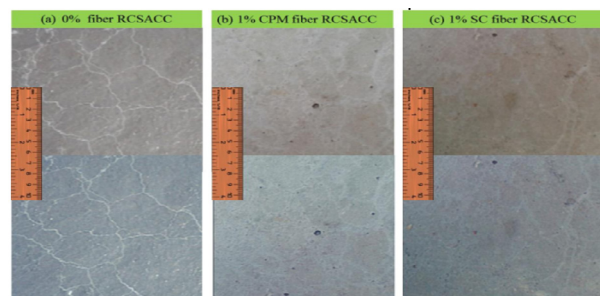


Figure 3. Shrinkage cracking for different RCSACC specimens in a 2.7×2.7 cm area
Source: Authors

The introduction of a 1% fiber content obviously helped to control the crack width in comparison with the control specimen (Figure 4). The crack width was reduced by an average of 30.89% and 51.75% with the introduction of 1% CPM and SC fiber content, respectively. As stated in the ACI 224R.01 standard (ACI Committee, 2011), a width between 0.1 and 0.3 mm is acceptable for the cracks provoked during plastic shrinkage. However, this requirement was not met by the control sample, unlike the 1% fiber-reinforced samples.

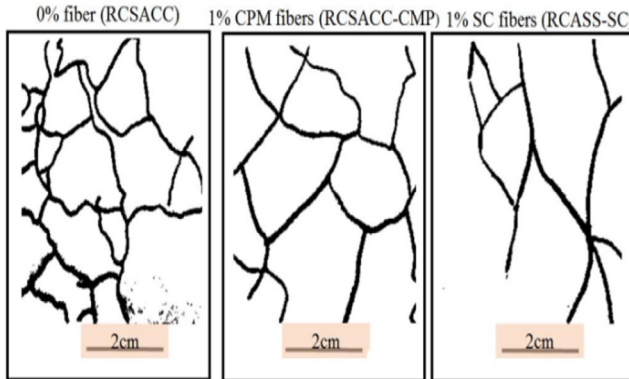


Figure 4. Shrinkage in different types of concrete (drawn in tracing paper from a printed image)
Source: Authors

Table 5 summarizes the characteristics of the cracks found in the samples with CPM and SC fibers.

Table 5. Crack characteristics of the reinforced RSACC

Concrete type	Total cracks (%)	Aver. crack width (mm)	Crack reduction (%)	Fiber content
RCSACC	11.40	1	-	0%
RCSACC-CMP	9.15	0.21	30.89	1%
RCSACC-SC	5.90	0.12	51.75	1%

Source: Authors

Figure 5 shows the shrinkage over 14 days of curing. The shrinkage of the RCSACC-CPM and RCSACC-SC samples differed from that of the RCSACC. The average shrinkage of the fiber-reinforced concrete (FRC) was larger than that of

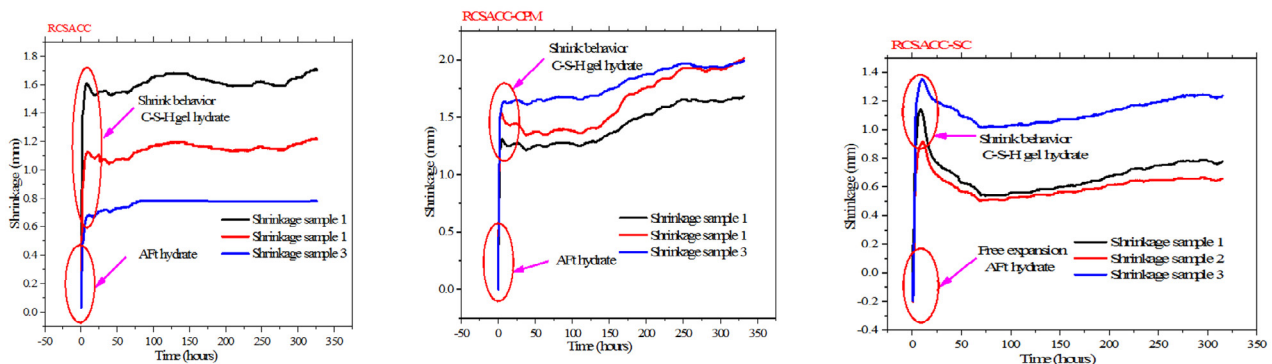


Figure 5. 14 days of free shrinkage in RCSACC with 0%, 1% CPM, and 1% SC fiber content
Source: Authors

the control sample. This may be because, when the fiber is added into the mixture, the microstructure is not as dense as that of the RCSACC with natural fine aggregate. Moisture can thus evaporate and migrate out of the sample more easily. The introduction of steel fibers in RCSACC reduces the strain during shrinkage, regardless of the fiber type. SC fibers reduce the shrinkage considerably. The development of RCSACC has two stages: rapid growth during the early hours of curing, when more than 86% of the total shrinkage takes place; and a slow development after 8 h.

Appearance of color and cracks after heating

Figure 6 shows the samples' variations in color, crack spreading, and spalling. In the RCSACC-CPM and RCSACC-SC samples exposed to 100, 200, and 300 °C, no large-scale spalling took place. CPM and SC helped to stop the spalling of the concrete when exposed to heat. In the control sample, the inner pore pressures are not released, leading to large-scale spalling. In contrast, in the samples with fibers, as the temperature rises, canals are formed on the bed of the fibers. These serve as a corridor to let compressed air escape and thereby reduce spalling through decreasing pore pressure.

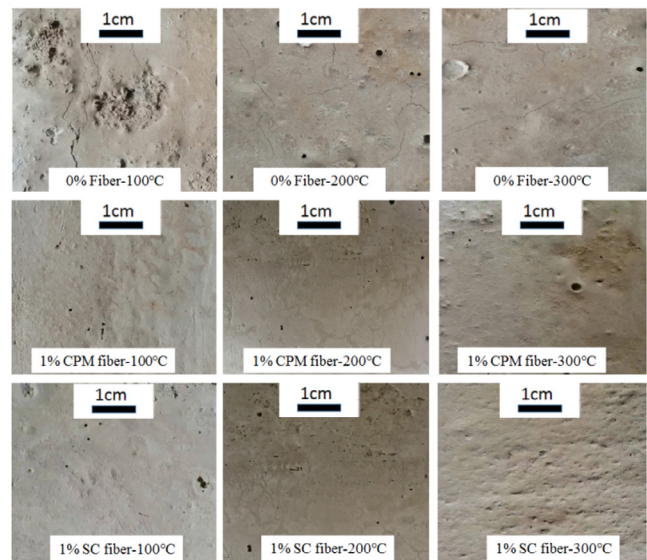


Figure 6. Exterior surface of the different RCSACC samples after exposure to a heat treatment
Source: Authors

Ultrasonic testing

The time required to transmit a pulse and the magnitude values from peak to peak, as obtained from the ultrasonic waveform (UW), are shown in Figure 7.

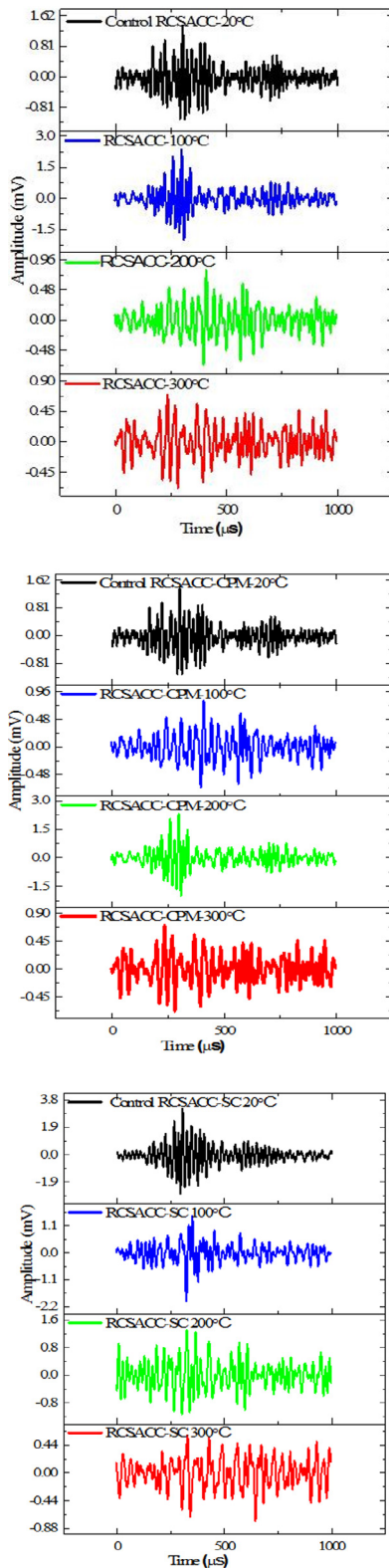


Figure 7. Ultrasonic waveforms

Source: Authors

As a result of exposure to elevated temperatures, the arrival time increased and the magnitude for the RCSACC sample decreased after being exposed to 100 and 200 °C. At 300 °C, the arrival time and magnitude decreased for the RCSACC-CPM and RCSACC-SC samples (Table 6). This evinces the presence of cracks caused by dehydration as the temperature increases.

Table 6. Ultrasonic wave analysis

	Samples	Aver. arrival time (μs)	Aver. amplitude (mV)	Change in amplitude (mV)
20 °C Before heating	RCSACC	300	3.35	
	CPM	296.7	2.33	
	SC	304	3.19	
100 °C After heating	RCSACC	296.7	2.33	1.02
	CPM	300.4	1.6	0.97
	SC	349.6	1.5	1.69
200 °C After heating	RCSACC	407.9	0.7	2.56
	CPM	408	0.79	1.54
	SC	325.2	1.3	1.89
300 °C After heating	RCSACC	311.9	0.8	2.52
	CPM	234.4	0.69	1.64
	SC	327.9	0.59	2.6

Source: Authors

All the samples, when tested at room temperature, exhibited a short transit time with a large magnitude, suggesting that, before heat exposure, the specimens had greater continuity and density. After the heating treatment, the difference between the exposed and unexposed specimens reflected the internal characteristics of the different RCSACCs. The waveform change could originate from waves spreading and coming into contact with many pores and microcracks. The attenuation was well explained by the presence of microcracks on the surface, which emerged as the temperature increased.

Compressive strength

Figure 8 shows the failure patterns of each specimen under compressive testing. The maximum strength was recorded for the samples at room temperature; they exhibit wide and significant spalling as well as characteristic cracks at higher temperatures. The specimen cracks were significant because they resulted from an applied load. Although lower strength and negligible cracking were observed in the samples heated to 100-300 °C, they performed adequately during the test due to the initial cracking caused by the heat. Moreover, the RCSACC-CPM and RCSACC-SC samples, when heated above 100 °C, exhibited an impressively large propagation of cracks and significant spalling, an evidence of the poor compactness between the different component matrices.

Adding CPM and SC fibers to RCSACC enhances some engineering properties after heat exposure. At room

temperature, a 3.6% increase in strength was recorded after adding 1% CPM; at 100 °C, 32.03% of the strength was retained. However, the introduction of 1% SC negatively impacted the sample’s compressive strength.

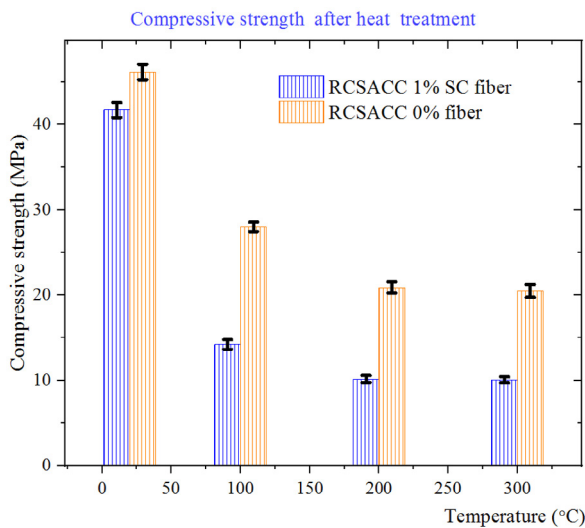
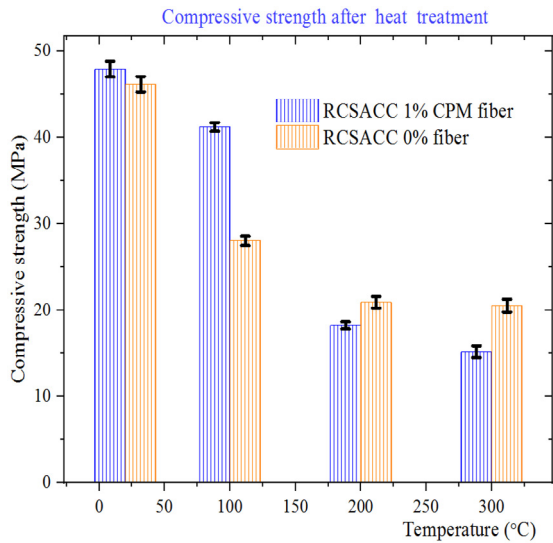


Figure 8. Strength of the fiber-reinforced concrete
Source: Authors

Flexural strength

The cracks observed in the reinforced samples during flexural testing are quite different from those of the control. CPM and SC resist the spread of the cracks uniformly. This suggests that crack propagation will concentrate in the zones with fewer fibers. Figure 9 shows that the FRC containing 1% SC has the highest flexural strength, greater than that of the sample with 1% CPM. The RCSACC-SC specimens showed a better flexural strength capacity because of the enhanced bond formed by the corrugations; as a consequence, the steel fibers could bridge small cracks more quickly. When cracks appeared, the corrugations remained solidly embedded on each side, acting as stress transfer media. When the maximum bond strength was reached, the pull-out

effect fully activated, allowing the adjacent fibers to delay the growth of the cracks. However, there was no significant difference between the strength of the control and that of the FRC with 1% CPM fiber exposed to 300 °C.

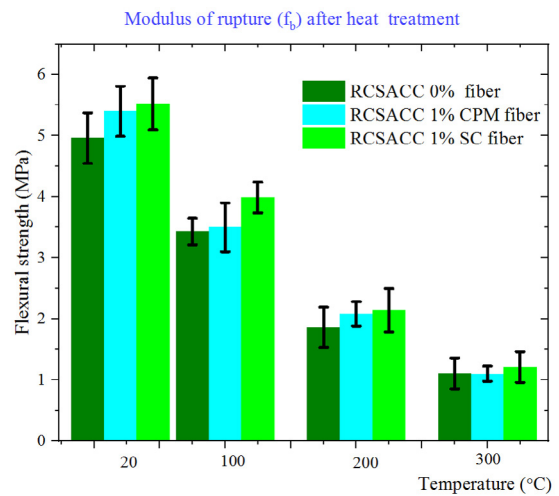


Figure 9. Flexural strength values
Source: Authors

Figure 10 shows the fracture deflection (f_{bb}) of the three types of RCSACC at different temperatures. For RCSACC-CPM, between 20 and 300 °C, there was a gradual difference in f_{bb}. The f_{bb} of the SC fibers varied greatly with temperature. A higher fracture deflection means more and longer cracks, as well as greater damage to the RCSACC sample. CPM fibers have a lower individual volume and can be more evenly distributed in the RCSACC. In contrast, the large volume of SC fibers and their corrugated structure make an even distribution more difficult.

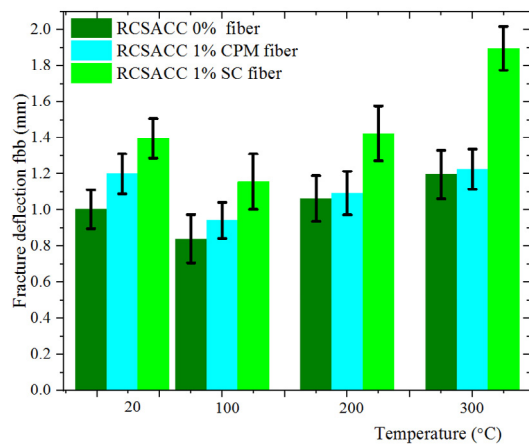


Figure 10. Fracture deflection
Source: Authors

At a normal temperature of 20 °C, the strength of the two FRCs was higher than that of the control sample, and there was little difference in f_{bb}. In a high-temperature environment, the structure of RCSACC-SC was destroyed. It is important to highlight that uneven SC fibers cause a greater f_{bb}. In addition, although their corrugated structure

macroscopically supports the flexural strength of RCSACC, SC fibers' ability to bond with RCSACC is greatly reduced. This indicates, to a certain extent, that the structure of RCSACC-SC is loose, which is another reason for the increase in deflection.

Figure 11 shows the load displacement curves of RCSACC-CPM and RCSACC-SC. The latter (Figure 11b) shows cracks when loaded, and its behavior evidence softening. It has a higher flexural strength than RCSACC-CPM (Figure 11a), exhibiting hardening.

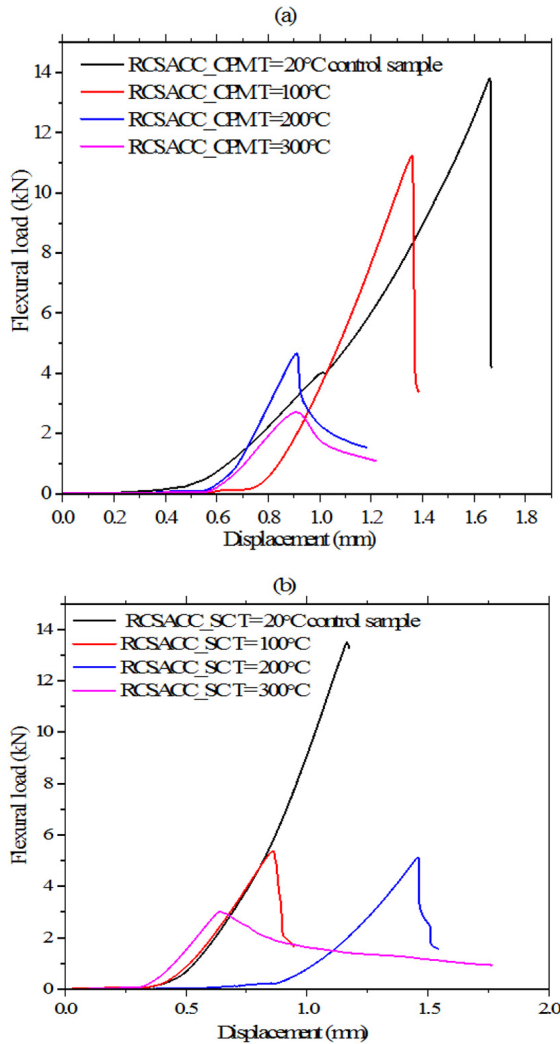


Figure 11. Load displacement curves of the samples with CMP and SC fibers at various temperatures
Source: Authors

MIP and SEM observations

Pore size curves are shown in Figure 12. The pore size of RCSACC-CPM and RCSACC-SC gradually increased with increasing temperature, and high temperatures promoted the deterioration of the microscopic pore structure. The microscopic observation of RCSACC-SC showed a higher mercury intrusion in the 100-1000 nm pore range when compared to RCSACC-CPM, which indicates that the

addition of steel fibers effectively emptied the 200-1000 nm pore size range, resulting in increased porosity.

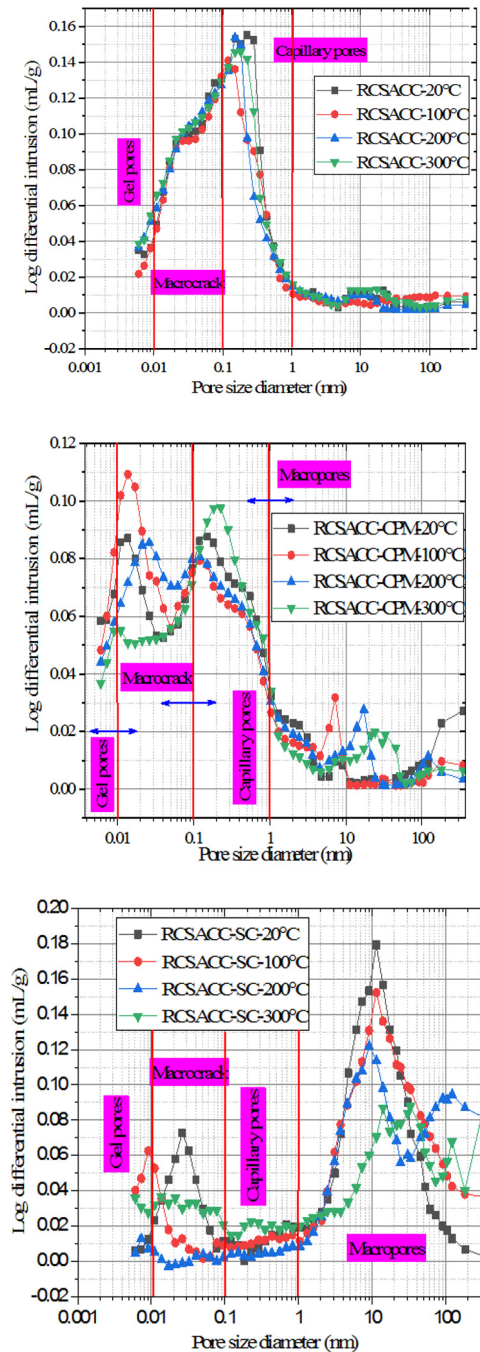


Figure 12. Pore structure results
Source: Authors

The sample reinforced with CPM steel fibers had a more constant increase in pore size distribution (PSD) as the temperature increased, in comparison with the control and the RCSACC-SC sample. Figure 13 shows that RCSACC is more compact at room temperature, which evidences the better homogeneity of the different matrices. Above 100 °C, RCSACC-CPM and RCSACC-SC exhibited a less compact internal structure, with the gradual appearance of macro-

and microcracks and pores as the temperature approached 300 °C. Numerous pores were observed in the different samples at 300 °C.

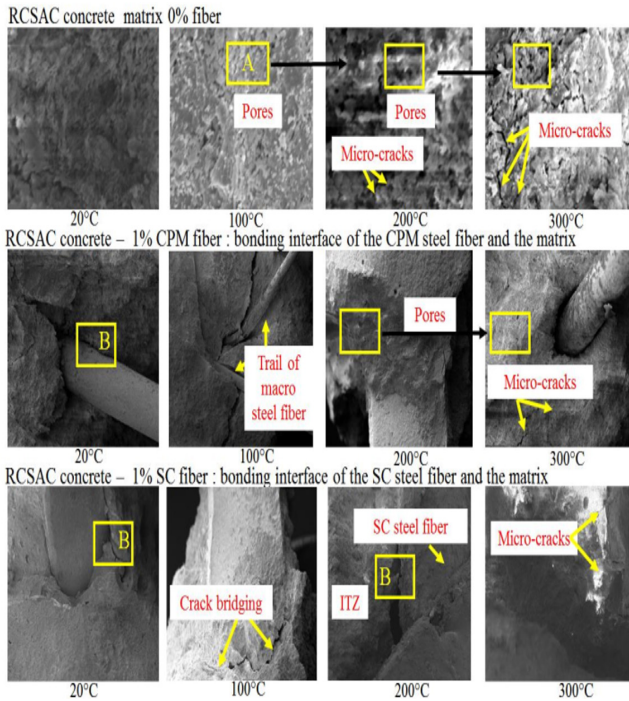


Figure 13. Different RCSACC samples as viewed through SEM
Source: Authors

A large number of pores and microcracks was observed in RCSACC-SC at 100 °C, mainly due to the crystalline transformation of the hydration products. Steel fibers exhibit an interwoven fiber network, which causes a significant increase in the flexural strength of fiber-reinforced RCSACC after high-temperature treatment.

Discussion

Significance of the results

When fiber is added to the mixture, the microstructure is not as dense as that of RCSACC with natural fine aggregate. This differs from literature reports of increased microstructure integrity under dry conditions (Abdulaziz *et al.*, 2020; Kaczmarek *et al.*, 2021), as well as from other works highlighting the increased failure of RCSACC microstructures after high-temperature exposure (Jacek *et al.*, 2021). Increased microstructure failure may affect the strength of the samples and their ability to resist high-temperature exposure (Abbass *et al.*, 2022). Given their ideal aspect ratio, the use of CPM and SC steel fibers in this study facilitated a more effective evaporation and migration of moisture out of the sample in comparison with hooked-end steel fibers, which have a significantly higher failure rate (Bibiana *et al.*, 2017; Ferdous *et al.*, 2018).

In general, fibers can bridge cracks and contribute to mitigating shrinkage cracking (Amin *et al.*, 2022). Our results show the effectiveness of CPM and SC fibers in restraining the shrinkage of the mixture. Adding these materials to RCSACC slightly improved the strength of the sample when compared to other steel fibers with higher aspect ratios (An *et al.*, 2017). Temperature was seen to be associated with changes in the suitability of RCSACC-CPM and RCSACC-SC at multiple scales. However, it was clear that adding a 1% steel fiber content was beneficial for flexural strength and crack expansion (*i.e.*, FRC containing 1% SC exhibited the highest flexural strength). RCSACC-SC showed the highest normalized strengths at all temperatures. This suggests that the brittleness decreased at high temperatures, whereas the ratio of flexural to compressive strength (F/C) increased with increasing temperature.

This study suggests that adaptive SC or CPM fibers may allow RSACC to resist high-temperature exposure. The strength ratio data suggest that the brittleness decreased with increasing temperature regardless of the type of fiber used. The normalized flexural strength generally decreased above 100 °C. For the SC specimens, the normalized flexural strength was much greater than that of the other two types. Our results highlight the potential for increasing the flexural strength of RCSACC by adding 1% SC or CPM fiber content to structures susceptible to heat exposure (Bang *et al.*, 2022). This addition increased the strength at 20 °C. Heating weakened the compressive strength of RCSACC with 1% SC more than it weakened that of RCSACC-CPM. For the latter, heating created pores in the structure (internal voids), which led to the unbonding of the aggregate, CPM fibers, and RCSAC paste that constitute the matrix. This, in turn, weakened, resulting in reduced compressive strength.

The samples exposed to 100 °C exhibited a compressive strength 6.7 MPa lower than that at 20 °C. Previous research (Dong *et al.*, 2022) found that the primary chemical decomposition product is generated after extended exposure to elevated temperatures. This was confirmed by the observed compressive strength reduction and the increase in the number of capillary pores, as well as in the length and width of the microcracks. RCSACC-CPM's flexural strength was lower than that of RCSACC-SC. However, in comparison with the control, there was an increase in flexural strength as the temperature rose. An increase in the load-bearing capacity and the ductility of the sample was observed in the FRC samples after extended heat treatment. RCSACC-SC, with a significant L/D value, increased its ability to resist crack propagation, given the large bonding area of SC fibers with the surrounding matrix (mortar). The specimens made with steel fibers showed a higher displacement resistance capacity and a high tensile strength. This observation agrees with previous research (Abdulkader *et al.*, 2017).

Adding SC fibers or CPM improved the flexural strength at elevated temperatures. The SC fibers increased the

flexural tensile strength of the sample after exposure in comparison with the control. FRC showed a post-exposure flexural traction strength comparable to that of RCSACC before exposure. RCSACC-CPM had a substantially greater load-bearing capacity after the treatment when compared to the control. RCSACC-CPM and RCSACC-SC introduced a pseudo-plastic state, suggesting that they could play a positive role in structures built with RCSACC that are susceptible to heat exposure.

Conclusions

According to the results and the analysis, the following conclusions can be drawn:

1. Ultrasonic wave testing could serve as a quick tool for monitoring and predicting the behavior of RCSACC at high temperatures; after extended conditioning, weakened properties were detected. Ultrasonic wave tests found that the quality of the samples was seriously compromised beyond 100 °C, leaving only RCSACC-SC in suitable condition. With the addition of 1% steel fiber content, the crack width was decreased by 72-93%. In RCSACC-SC, the cracks were almost eliminated, whereas the control showed much wider cracks.
2. The addition of 1% SC reduces the workability and, as a result, the slump of RCSACC. This could be due to the D/L value of SC fibers. The aspect ratio of these fibers caused the RCSACC and sand to wrap around them, creating sturdy fiber-matrix bonds. The ultimate result of this bonding was reduced strength.
3. The aforementioned addition improves the mechanical properties of RCSACC after heat exposure depending on the type of fiber used. At 20 °C, there was a 3.6% increase in compressive strength for RCSACC-CPM, and its flexural strength improved by 8.14%. Overall, a 1% fiber content enhanced the flexural strength of RCSACC.
4. SC and CPM steel fibers aid in transferring stress, which results in increased strength after the treatment when compared to the control. At 100 °C, RCSACC-CPM showed an average compressive strength of 41.2 MPa and a flexural strength of 3.5 MPa, compared to the 28 and 2.43 MPa values obtained by the control. The SC and CPM steel fibers enhanced the samples' ductility.
5. SEM and MIP observations revealed that, at the conditioning temperatures, cracks tended to propagate throughout the RCSACC matrix. The pore size increased as the temperature increased, regardless of the sample, resulting in reduced strength.

Overall, based on these data, a 1% CPM or SC steel fiber content cannot be regarded as an adequate addition, since the paste did not bond sufficiently with these materials, resulting in a more porous concrete with many microcracks, leading to poor performance after conditioning.

Acknowledgements

The authors gratefully acknowledge the financial support received from the Key Laboratory of Green Building Materials (2023GBM03), the Shandong Provincial Higher Education Youth Innovation Team Program of China (2022KJ284), the 111 Project of International Cooperation on Advanced Cement-Based Materials (No. D17001), and the Taishan Scholars Program of China.

CRedit author statement

Jean Jacques Kouadjo Tchekwagep conceived the idea and did the background research. Yiping Qiu and Shifeng Huang collected the data, developed the workflow, and performed the assessment. Shoude Wang and Xin Cheng supervised the research and provided critical feedback. Jean Jacques Kouadjo Tchekwagep wrote the main part of the manuscript, to which all authors contributed.

Conflicts of interest

We declare that there are no conflicts of interest.

References

- ACI Committee (2011). *ACI 214R-11 – guide to evaluation of strength test results of concrete*. American Concrete Institute.
- Abbass, A. A., Abid, S.R., Ali, S. H., Al-Sarray, M. L. J., Murali, G., and Nader, I. A. (2022). Post-high-temperature exposure repeated impact response of steel-fiber-reinforced concrete. *Buildings*, 12, 1364. <https://doi.org/10.3390/buildings12091364>
- Abdulaziz, A., and Yousef R. A. (2022). Strength, durability and shrinkage behaviours of steel fiber reinforced rubberized concrete. *Construction and Building Materials*, 345, 128295. <https://doi.org/10.1016/j.conbuildmat.2022.128295>
- Abdulkader E M., Roland L., and Salem G. N. (2017). Mechanical performance of steel fiber reinforced self-compacting concrete in panels. *Procedia Engineering*, 196, 90-96. <https://doi.org/10.1016/j.proeng.2017.07.177>
- Afroughsabe, V., Biolzi, L., and Ozbakkaloglu, T. (2016). High-performance fiber-reinforced concrete: A review. *Journal of Materials Science*, 51, 6517-6551. <https://doi.org/10.1007/s10853-016-9917-4>
- Aguilar, M. T. P., Bezerra, A. C. S., De Figueiredo, M. A. L., Melo, P. G., Silva, M. J., Oliveira, S. N., Oliveira, L. L. M. S., Resende, D. S., and Silva, N. J. T. (2016). Evaluation of sample preparation parameters in the compressive strength of cementitious composites. *Materials Science Forum*, 869, 93-97. <https://doi.org/10.4028/www.scientific.net/MSF.869.93>
- Ahmed N. E. (2021). EGYGene GelAnalyzer4: A powerful image analysis software for one dimensional gel electrophoresis. *Journal of Genetic Engineering and Biotechnology*, 19, 18. <https://doi.org/10.1186/s43141-020-00114-x>

- Aluko, O. G., Kadir, M. A. A., Yatim, J. M., and Yahya, K. (2020). A review of properties of bio-fibrous concrete exposed to elevated temperatures. *Construction and Building Materials*, 260, 11967. <https://doi.org/10.1016/j.conbuildmat.2020.119671>
- Amin, M. N., Ahmad, W., Khan, K., and Ahmad, A. (2022). Steel fiber reinforced concrete: A systematic review of the research progress and knowledge mapping. *Materials*, 15, 6155. <https://doi.org/10.3390/ma15176155>
- An, L. H., and Ekkehard F. (2017). Influence of steel fiber content and aspect ratio on the uniaxial tensile and compressive behavior of ultra high performance concrete. *Construction and Building Materials*, 153, 790-806. <https://doi.org/10.1016/j.conbuildmat.2017.07.130>
- Aravinthan, T., Ferdous, W., Ghabraie, K., Manalo, A., and Van, E. G. (2018). Evaluation of an innovative composite railway sleeper for a narrow-gauge track under static load. *Journal of Composites for Construction*, 2, 04017050-1-13. [https://doi.com/10.1061/\(ASCE\)CC.1943-5614.0000833](https://doi.com/10.1061/(ASCE)CC.1943-5614.0000833)
- Augusto, C. S. B., Elaine, C. S. C., Maria, T. P. A., Priscilla, S. M., Paulo, R. R. S. J., and Paulo, R. C. (2019). Effect of high temperature on the mechanical properties of steel fiber-reinforced concrete. *Fibers*, 7(12),100. <https://doi.org/10.3390/fib7120100>
- Azzabi, M., Banthia, N., and Pigeon, M. (1993). Restrained shrinkage cracking in fiber-reinforced cementitious composites. *Materials and Structures*, 26, 405-413. <https://doi.org/10.1007/BF02472941>
- Barreto, R. R., Bezerra, A. C. S., Maciel, P. S., Soares, J. P. R. R., Silva Neto, J. T., and Siqueira Corrêa, E. C. (2019). Thin slabs made of high-performance steel fibre-reinforced cementitious composite: Mechanical behaviour, statistical analysis and microstructural investigation. *Materials*, 20, 3297. <https://doi.org/10.3390/ma12203297>
- Bai, Y., Ferdous, W., Manalo, A., Mendis, P., and Ngo, T. D. (2019). New advancements, challenges and opportunities of multi-storey modular buildings: A state-of-the-art review. *Engineering Structure*, 83, 883-893. <https://doi.org/10.1016/j.engstruct.2019.01.061>
- Bang, Y. L., Jeong-Il C., Se-Eon P., and Yun, Y. K. (2022). Flexural behavior of composite beams of Kagome truss and fiber-reinforced cementitious composites. *Construction and Building Materials*, 361, 129653. <https://doi.org/10.1016/j.conbuildmat.2022.129653>
- Bibiana, L., Facundo, I., Gonzalo, R., Graciela, G., and Raúl Z. (2017). Steel fibers pull-out after exposure to high temperatures and its contribution to the residual mechanical behavior of high strength concrete. *Construction and Building Materials*, 163, 571-585. <https://doi.org/10.1016/j.conbuildmat.2017.12.129>
- Bjegović, D., Baričević, A. R., Pezer, M., Serdar, M., and Štirmir, N. (2015). Shrinkage behaviour of fibre reinforced concrete with recycled tyre polymer fibres. *Civil Engineering Applications of Polymer Composites*, 2015(1), 145918. <https://doi.org/10.1155/2015/145918>
- Błaszczczyński, T., and Przybylska, M. (2015). Steel fibre reinforced concrete as a structural material. *Procedia Engineering*, 11-12, 44-50 <https://doi.org/10.1016/j.proeng.2015.10.037>
- Chang, K. H., Wang, W., Wang, H. Y., and Wang, S. Y. (2020). Effect of high temperature on the strength and thermal conductivity of glass fiber concrete. *Construction and Building Materials*, 245, 118387. <https://doi.org/10.1016/j.conbuildmat.2020.118387>
- Chalioris, C. E., Kosmidou, P. M. K., and Karayannis, C. G. (2019). Cyclic response of steel fiber reinforced concrete slender beams; An experimental study. *Materials*, 12(9), 1398. <https://doi.org/10.3390/ma12091398>
- Cheng, X., Che, J., Liu, H., Liu, N., and Zhang, M. (2020). Mechanical performances of concrete produced with desert sand after elevated temperature. *International Journal of Concrete Structures and Materials*, 14, 26. <https://doi.org/10.1186/s40069-020-00402-3>
- Cheng, X., Huang, S., Kouadjo, J. J. T., Mukhopadhyay, A. K., and Wang, S. (2020a) Compressive strength of rapid sulfoaluminate cement concrete exposed to elevated temperatures. *Ceramics-Silikáty*, 64(3), 1-10. https://www.irsm.cas.cz/materialy/cs_content/2020_doi/Tchekwagep_CS_2020_0012.pdf
- Cheng, X., Huang, S., Kouadjo, J. J. T., Mukhopadhyay, A. K., and Wang, S. (2020b). Strengths of sulfoaluminate cement concrete and ordinary portland cement concrete after exposure to high temperatures. *Ceramics-Silikáty*, 64(2), 1-9. https://www2.irsm.cas.cz/materialy/cs_content/2020_doi/Tchekwagep_CS_2020_0019.pdf
- Cheng, X., Huang, S., Kouadjo, J. J. T., Mukhopadhyay, A. K., and Wang, S. (2021). The impact of extended heat exposure on rapid sulphoaluminate cement concrete up to 120°C. *Periodica Polytechnica Civil Engineering*, 65(2), 588-607. <https://doi.org/10.3311/PPci.17122>
- Dong D., Lingchao L., Na C., Piqi Z., Xuecheng W., Yongbo H., and Zixu Z. (2022). Ternessite-calcium sulfoaluminate cement: Preparation and hydration. *Construction and Building Materials*, 344,128187. <https://doi.org/10.1016/j.conbuildmat.2022.128187>
- Ferdous, W., Ghazlan, A., Mendis, P., Manalo, A., Ngo, T. D., and Nguyen, K. T. Q. (2018). Effect of fire-retardant ceram powder on the properties of phenolic-based GFRP composites. *Composites Part B Engineering*, 155, 414-424. <https://doi.org/10.1016/j.compositesb.2018.09.032>
- Gashti, S. H., Sadrmomtazi, A., and Tahmouresi B. (2020). Residual strength and microstructure of fiber reinforced self-compacting concrete exposed to high temperatures. *Construction and Building Materials*, 230, 116969. <https://doi.org/10.1016/j.conbuildmat.2019.116969>
- Hong, S. G., Kang, S. H., Lee, J. H., and Moon, J. (2017). Microstructural investigation of heat-treated ultra-high-performance concrete for optimum production. *Materials*, 10(9), 1106. <https://doi.org/10.3390/ma10091106>
- Jacek, S., Konrad, A. S., Łukasz, K., Mariusz, S., and Sebastian, M. (2021). Impact of elevated temperatures on strength properties and microstructure of calcium sulfoaluminate paste. *Materials*, 14(22), 6751. <https://doi.org/10.3390/ma14226751>
- Kaczmarek, Ł., Miszczak, S., Sodoł, K. A., Stegliński, M., and Szer, J. (2021). The Influence of elevated temperatures on strength properties and microstructure of calcium sulfoaluminate paste. *Materials*, 14, 6751. <https://doi.org/10.3390/ma14226751>

- Kohoutková, A., and Novák, J. (2017). Fiber reinforced concrete exposed to elevated temperature. *Materials Science and Engineering*, 1, 012045. <https://doi.org/10.1088/1757-899X/246/1/012045>
- Li, L. (2019). Stress-rupture of fiber-reinforced ceramic-matrix composites with stochastic loading at intermediate temperatures. Part I: Theoretical analysis. *Materials*, 12(19), 435-458. <https://doi.org/10.1007/s41779-020-00549-y>
- Li, Y., Nguyen, H. T. N., and Tan, K. H. (2021). Shear behavior of fiber-reinforced concrete hollow-core slabs under elevated temperature. *Construction and Building Materials*, 275, 121362. <https://doi.org/10.1016/j.conbuildmat.2020.121362>
- Li, Y., Tan, K. H., and Yang, E. (2020). Flexural behavior of ultra-high performance hybrid fiber reinforced concrete at the ambient and elevated temperature. *Construction and Building Materials*, 250, 118487. <https://doi.org/10.1016/j.conbuildmat.2020.118487>
- Mehta, P. K., and Monteiro, P. J. M. (2006). *Concrete: Microstructure, properties, and materials* (3rd ed). McGraw-Hill.
- Michels, J., Scherer, J., and Zwicky, D. (2016). Structural strengthening of concrete with fiber reinforced cementitious matrix (FRCM) at ambient and elevated temperature – Recent investigations. *Advances in Structural Engineering*, 17(12), 1785-1799. <https://doi.org/10.1260/1369-4332.17.12.1785>
- Tanyildizi, H., and Yonar, Y. (2016). Mechanical properties of geopolymer concrete containing polyvinyl alcohol fiber exposed to high temperature. *Construction and Building Materials*, 216, 381-387. <https://doi.org/10.1016/j.conbuildmat.2016.09.001>
- Venkatesh, K., and Wasim, K. (2011). Thermal and mechanical properties of fiber reinforced high performance self-consolidating concrete at elevated temperatures. *Cement and Concrete Research*, 41(11), 1112-1122. <https://doi.org/10.1016/j.cemconres.2011.06.012>